Ras Catalyzes GTP Hydrolysis by Shifting Negative Charges from γ- to β-Phosphate As Revealed by Time-Resolved FTIR Difference Spectroscopy[†]

Christoph Allin and Klaus Gerwert*

Lehrstuhl für Biophysik, Ruhr-Universität Bochum, D-44780 Bochum, Germany

Received July 24, 2000; Revised Manuscript Received January 9, 2001

ABSTRACT: FTIR difference spectroscopy has been used to determine the molecular GTPase mechanism of the small GTP binding protein Ras at the atomic level. The reaction was initiated by the photolysis of caged GTP bound to Ras. The addition of catalytic amounts of the GTPase activating protein (GAP) reduces the measuring time by 2 orders of magnitude but has no influence on the spectra as compared to the intrinsic reaction. The reduced measuring time improves the quality of the data significantly as compared to previously published data [Cepus, V., Scheidig, A., Goody, R. S., and Gerwert, K. (1998) *Biochemistry 37*, 10263−10271]. The phosphate vibrations are assigned using ^{18}O-labeled caged GTP. In general, there is excellent agreement with the results of Cepus et al., except in the $\nu_a(\alpha\text{-PO}_2^-)$ vibration assignments. The assignments reveal that binding of GTP to Ras induces vibrational uncoupling into mainly individual vibrations of the α-, β-, and γ-phosphate groups. In contrast, for unbound GTP, the phosphate vibrations are highly coupled and the corresponding absorption bands are broader. This result indicates that binding to Ras forces the flexible GTP molecule into a strained conformation and induces a specific charge distribution different from that in the unbound case. The binding causes an unusual frequency downshift of the GTP β-PO$_2^-$ phosphate vibration, whereas the α-PO$_2^-$ and γ-PO$_3^{2-}$ phosphate vibrations shift to higher wavenumbers. The frequency downshift indicates a lowering of the bond order of the nonbridged P−O bonds of the β-phosphate group of GTP and GDP. The bond order changes can be explained by a shift of negative charges from the γ- to the β-oxygens. Thereby, the GTP charge distribution becomes more like that in GDP. The charge shift appears to be a key factor contributing to catalysis by Ras in addition to the correct positioning of the attacking water. Ras appears to increase the negative charge at the *pro-R* β-oxygen mainly by interaction of Mg^{2+} and at the *pro-S* β-oxygen mainly by interactions of the backbone NHs of Lys 16, Gly 15, and Val 14. The correct positioning of the backbone NHs of Lys 16, Gly 15, and Val 14, and especially the Lys 16 side chain, of the structural highly conserved phosphate binding loop relative to β-phosphate therefore seems to be important for the catalysis provided by Ras.

The guanine nucleotide binding protein Ras plays a central role in the transduction of growth signals from the plasma membrane to the nucleus (*1*). It acts as a switch cycling between an active GTP[1]-bound and an inactive GDP-bound form. Such a switch mechanism is found in pathways involved in cell proliferation, signal transduction, differentiation, protein synthesis, and protein transport. Therefore, understanding the detailed GTPase mechanism of Ras might provide a paradigm for many similar processes.

GDP-bound Ras is activated by guanine nucleotide exchange factors (Ras-GEFs). In the GTP-bound form, Ras interacts with its effector Raf. Binding of the effector activates a kinase cascade, which transduces the external signal via a series of phosphorylations to the nucleus. The effector binding is terminated by hydrolysis of protein-bound GTP to GDP. Ras exhibits a very slow intrinsic hydrolytic activity, which is significantly increased by the interaction with GTPase activating proteins (GAPs) (*2*). The molecular GTPase mechanism of Ras is particularly relevant since oncogenic Ras mutants appear to be involved in 25−30% of all human tumors. The molecular defect in these mutant proteins stems from the inability of Ras to hydrolyze GTP (*3*). The longer Ras remains in its functionally active state, the longer the signal will be transmitted and amplified, which finally results in uncontrolled cell growth.
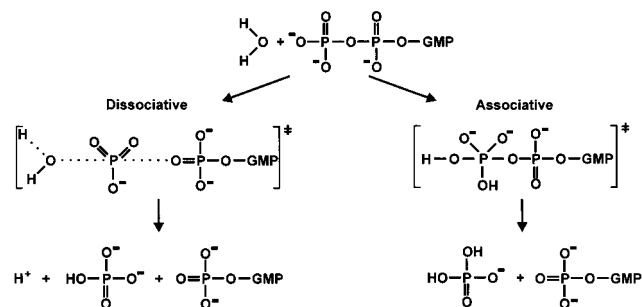
A milestone for the understanding of the GTPase mechanism was the elucidation of structural models for Ras in its active and inactive states by X-ray crystallography (*4*, *5*). However, to prevent GTP hydrolysis during data acquisition, slowly hydrolyzing GTP analogues such as GppNHp have to be used to stabilize the active state. Because the most important bond is significantly changed in the analogues, the structural models might not optimally mimic the catalytic center of the protein. In another approach, the Laue crystallographic approach was used to determine the Ras·GTP structure, but yielded lower structural resolution than the monochromatic technique (*6*). The resolution was signifi-

[1] Abbreviations: caged GTP, P^3-1-(2-nitrophenyl)ethylguanosine 5′-*O*-triphosphate; DTT, dithiothreitol; FTIR, Fourier transform infrared; GTP, guanosine 5′-triphosphate; GDP, guanosine 5′-diphosphate; GppNHp, guanosine 5′-(β,γ-imidotriphosphate); MES, 2-(*N*-morpholino)ethanesulfonic acid; NF1-333, catalytic domain of the product of the neurofibromatosis type 1 gene; P$_i$, inorganic phosphate.

Scheme 1:   Comparison of the Dissociative and Associative Transition State

Scheme 2:   Release of GTP from Caged GTP

(Scheme 2). For the investigations, the reaction was started by flash photolysis at 308 nm with an excimer laser. After cleavage of the photolabile protecting group, GTP is recognized as a substrate by Ras and hydrolyzed. The photolysis and hydrolysis reactions were monitored by time-resolved FTIR difference spectroscopy as established by Cepus et al. (10). The time-resolved difference spectra reflect all reactions taking place during hydrolysis by the IR absorbance changes of the involved groups. To accelerate the GTPase reaction, catalytic amounts of NF1-333 (2) were added to the solution. Compared to that of the results of Cepus et al. (10), the quality of the hydrolysis difference spectra is now markedly improved due to the reduction of the measuring time by 2 orders of magnitude. This significantly reduces the disturbing influence of baseline drift. The difference spectra are almost unaltered by the catalytic amounts of NF1-333. The IR absorption bands of the α- and γ-phosphate group were assigned using α-^{18}O- and γ-^{18}O-labeled caged GTP. The β-phosphate vibrations were assigned using stereospecific (S_P) and (R_P) β-^{18}O-labeled caged GTP. For labeling of the released P_i, measurements were performed in $H_2^{18}O$. On the basis of the isotopic shifts due to the labeling, the assignments for the phosphate bands are now clear-cut. Binding to Ras induces localized phosphate vibrations in contrast to unbound GTP. The band assignments, their implications for the charge distribution in GTP and GDP due to Ras binding, and the implications for the GTPase mechanism will be discussed.
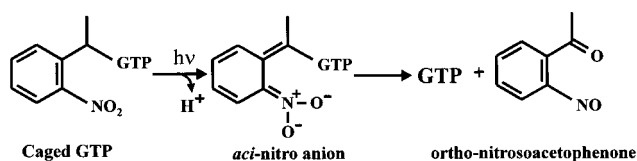
cantly improved by freezing the crystals and collecting data with monochromatic X-rays (7). However, freezing induces certain artificial structural changes, e.g., the catalytically active water molecules shift in their positions (7), but just these water molecules, especially water 175 (4), are proposed to be crucial for the mechanism of the GTPase reaction. Furthermore, the structural models of oncogenic mutants do not exhibit large structural changes when compared to the wild type structural models, and could not explain the dramatically lowered hydrolysis rate (8). There is also still a controversial debate about the fundamental question as to what extent the reaction proceeds via a dissociative or an associative mechanism (Scheme 1) (9). In a purely dissociative transition state, the $\beta-\gamma$ bridging bond is first split, and an instable metaphosphate species is produced, with negative charge moving from γ- toward the β-phosphate. In a purely associative mechanism, a pentacovalent transition state or intermediate is formed and negative charge accumulates on the γ-phosphate. Subsequently, the $\beta-\gamma$ bridging bond is cleaved. However, independent of the reaction pathway, finally charge is moved from the γ-PO_3^{2-} to the β-PO_3^{2-} group. In conclusion, it is possible that the fine details of interactions not resolved by X-ray crystallography might contribute significantly to the GTPase mechanism, and for this reason, additonal techniques are required to obtain this missing information.

In principle, vibrational spectroscopy can provide complementary information about bond orders, charge distribution, and H-bonding of individual groups. In addition, measurements are performed in solution at room temperature, allowing the investigated proteins to maintain their native conformations instead of being forced into specific conformations stabilized in the crystal. The crystalline state might also prevent conformational changes during the reaction. The first investigation on the GTPase mechanism of Ras by vibrational spectroscopy was reported by Cepus et al. (10). Using time-resolved FTIR difference spectroscopy, the GTPase reaction can be monitored in real time at atomic resolution. Then complementary Raman experiments by Wang et al. (11) and recently additional FTIR measurements by Du et al. (12) were also performed.

As compared to that of the first contribution by Cepus et al. (10), the quality of the data is now significantly improved. The active state is obtained by photolysis of caged GTP (Scheme 2). Caged GTP binds to Ras, but is not hydrolyzed (6). After irradiation of caged GTP, the *aci*-nitro anion of caged GTP is formed in less than 10 μs at room temperature (13). This intermediate decays in a rate-determining step to GTP and *o*-nitrosoacetophenone in the millisecond time range

MATERIALS AND METHODS

Wild type full-length H-Ras was prepared from *Escherichia coli* using the p*tac*-expression system as described previously (14). The ^{18}O-labeled phosphate was prepared from PCl_5 (Fluka) and $H_2^{18}O$ (99.1 at. % ^{18}O, Campro Scientific). [β,γ-$^{18}O,\gamma$-$^{18}O_3$]GTP was prepared from GDP (Fluka) by condensation of the phosphorimidazolidate of GDP with ^{18}O-labeled phosphate (15, 16). (R_P)-[β-^{18}O]GTP and (S_P)-[β-^{18}O]GTP were prepared from the S_P and R_P isomers of [β-S]GTP (17, 18). Caged GTP, caged [β,γ-$^{18}O,\gamma$-$^{18}O_3$]GTP, caged (S_P)-[β-^{18}O]GTP, and caged (R_P)-[β-^{18}O]-GTP were synthesized by esterification with 1-(2-nitrophenyl)-diazoethane following the procedure of Walker et al. (13). The mixture of caged [α-^{18}O]GTP and caged [γ-^{18}O]GTP was prepared starting with the sulfur analogue [γ-S]GTP (Boehringer Mannheim) which was esterified to S-caged and O-caged [γ-S]GTP (19). The isomers were separated by anion exchange chromatography on a DEAE column. O-caged [γ-S]GTP was hydrolyzed with $H_2^{18}O$ (18). The analysis of the product by mass spectrometry showed the incorporation of one ^{18}O atom. When a phosphatase was added to the released GTP, two peaks with approximately same height appeared in the spectrum at *m/z* 442 and 444. The appearance of the two peaks after treatment with

phosphatase is explained by unlabeled und singly labeled GDP after the cleavage of $P^{18}O^{16}O_2H$ and $P^{16}O_3H$ from GTP, respectively. ^{31}P NMR measurements of the labeled caged GTP was performed to clarify the position of the labeling. Different from the resonance lines for unlabeled caged GTP, the spectrum exhibited multiplets for the resonance lines of the α- and γ-phosphorus, whereas the β-phosphorus signal exhibited the expected triplet. It was concluded from these results that the product was a mixture of caged $[α-^{18}O]$GTP and caged $[γ-^{18}O]$GTP in a ratio of approximately 1:1. This stands in contrast to the former proposal by Cepus et al. (*10*), who assumed that the synthesis only leads to γ labeling. A similar observation was made by Connolly and Eckstein where the reaction of ATPαS resulted in a distribution of ^{18}O in the γ- and α-phosphorus groups in a ratio of approximately 2:1 (*17*). An explanation could be that a cyclic triphosphate is an intermediate during the reaction (*20, 21*).

The alkylation of GTP gives rise to diastereomers with a chiral center at the benzyl carbon (*13*). These diastereomers were not resolved for the investigations, but this should not affect the results since the focus of the work is on the assignment of GTP and GDP and not caged GTP phosphate vibrations.

The Ras·caged nucleotide complex was prepared as described previously (*10, 22*). For the FTIR measurements, 1 μL of the sample solution was prepared between two CaF_2 windows. The distance between these two windows was held at about 2.5 μm by a spacer ring made out of Mylar. The windows were fixed by a metal cuvette in the thermostated sample holder of the spectrometer. The sample solutions for the assessment of the photolysis reaction contained 10.0 mM Ras·caged nucleotide complex, 20 mM $MgCl_2$, 20 mM DTT, 200 mM MES (pH 6.0), and 12 vol % ethylene glycol. The sample solutions for the assessment of the GTPase reaction contained 10 mM Ras·caged GTP complex, 0.1 mM NF1-333, 20 mM $MgCl_2$, 20 mM DTT, 200 mM MES (pH 6.0), and 12 vol % ethylene glycol. Dithiothreitol was used to scavenge the reactive photolysis byproduct 2-nitroso-acetophenone. For measurements in $H_2^{18}O$, the sample solution was enriched in ^{18}O by repeated evaporation of added $H_2^{18}O$.

The FTIR measurements were performed on modified IFS 66v and IFS 66v/S spectrometers (Bruker, Karlsruhe, Germany) equipped with a mercury cadmium telluride (MCT) detector using the fast scan technique (*23*). The OPUS software (Bruker) was used for data acquisition. Spectra were collected in the double-sided forward−backward acquisition mode with a spectral resolution of 4 cm^{-1} and apodized with the Blackman−Harris three-term function. A zero-filling factor of 2 was used. The spectra were measured between 2000 and 950 cm^{-1} and analyzed by a global fit algorithm (*24, 25*) with one exponential term:

$$\Delta A(\nu,t) = \sum_i a_i(\nu)\, e^{-k_i \cdot t}$$

The global fit analysis provides amplitude spectra $a_i(\nu)$ and the rate constants k_i. The photolysis of caged GTP was performed at 308 nm using an LPX 240 XeCl excimer laser (Lambda Physics, Göttingen, Germany). A more detailed description of the experimental setup can be found elsewhere (*26*). The laser energy was between 90 and 120 mJ per flash

Scheme 3: Investigated Reactions
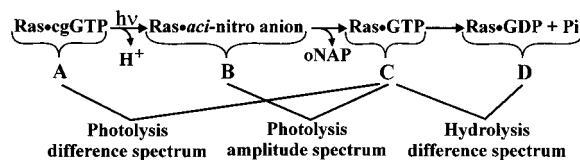
with a pulse duration of ∼20 ns. The conversion of caged GTP was checked by HPLC analysis using a reversed-phase C-18 column under ion pairing conditions with 50 mM potassium phosphate (pH 6.5), 5 mM tetrabutylammonium bromide, and 20% acetonitrile. For the investigation of the photochemical release of GTP, 30 flashes were applied to achieve 70−80% conversion of caged GTP to GTP in 90 ms. The chosen number of flashes was a compromise between the time of photolysis and the degree of conversion. The photolysis measurements with the Ras·caged GTP complex were performed at 260 K to inhibit the hydrolysis reaction. For the investigation of the GTPase reaction, 60 flashes were applied to achieve complete conversion of caged GTP to GTP. The measurements of the GTPase reaction were performed at 283 K. The hydrolysis difference spectra were calculated from the 400 averaged scans between 1 and 8 s after photolysis, representing the Ras·GTP state, and from the 800 averaged scans recorded between 48 and 62 s after photolysis, representing the Ras·GDP state. The amplitude and difference spectra were normalized to the bands between 1550 and 1300 cm^{-1}, where no change due to the isotopic labeling was observed.

RESULTS

After irradiation of caged GTP bound to Ras (Scheme 3, A), the *aci*-nitro anion of caged GTP (B) is formed. This intermediate decays to GTP (C) and *o*-nitrosoacetophenone (oNAP). The difference spectrum between A and C is called the photolysis difference spectrum. The decay of the Ras· *aci*-nitro anion intermediate (B) to Ras·GTP (C) can be described by the single-exponential function $\Delta A(\nu,t) = a(\nu)e^{-kt}$. The corresponding amplitude spectrum $a(\nu)$ (i.e., the amplitude in dependence of cm^{-1}) of the rate constant k is called the photolysis amplitude spectrum. It represents the differences between B and C. After cleavage of the photo-labile protecting group, GTP hydrolysis takes place and the Ras·GDP complex and P_i are formed (D). The difference between C and D is called the hydrolysis difference spectrum.

Photolysis of the Ras·Caged GTP Complex. At 260 K, the decay of the *aci*-nitro anion to GTP can be resolved with the fast scan technique. The global fit analysis of the absorbance changes between 1800 and 950 cm^{-1} after photolysis of Ras-bound caged GTP yields a rate constant for the decay of the Ras·*aci*-nitro intermediate (Scheme 3, B to C) of 5 ± 1 s^{-1} at 260 K. In Figure 1, the corresponding photolysis amplitude spectrum (Scheme 3, C − B) of this rate constant is compared with the photolysis difference spectrum (Scheme 3, C − A). Negative bands in the spectra indicate disappearing bands of the initial state, and positive bands indicate appearing bands of the product (Ras·GTP). The photolysis difference spectrum (Figure 1) agrees well with the difference spectrum published by Cepus et al. (*10*), although slightly different conditions (buffer and pH) were
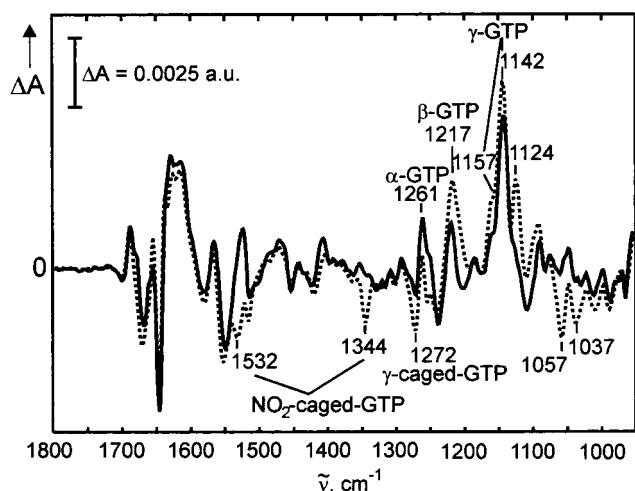
FIGURE 1: Photolysis amplitude spectrum (B − C) (—) and photolysis difference spectrum (A − C) (···) of the Ras·caged GTP complex at 260 K (see Scheme 3). The absorbance changes are normalized to the bands between 1800 and 1550 cm⁻¹. Deviations between the spectra reflect reactions from A to B [(B − C) − (A − C)] (see Scheme 3).

used. Most of the photolysis difference spectrum is in good agreement with the amplitude spectrum (Figure 1). This indicates that most of the molecular reactions occur during the decay of the *aci*-nitro anion to the Ras·GTP complex. The rate of formation of the *aci*-nitro anion is in the microsecond time range (*13*), so this process cannot be resolved with the fast scan technique. However, the *aci*-nitro anion decays with a rate in the millisecond time range, allowing resolution of this intermediate. The starting point for the photolysis difference spectrum (C − A) is the Ras·caged GTP state and for the photolysis amplitude spectrum (C − B) the *aci*-nitro anion state. The end point is in both cases the Ras·GTP state. Therefore, the deviations between these two spectra can be attributed to the structural differences between the Ras·caged GTP and Ras·*aci*-nitro anion species.

Significant differences between the two spectra are seen at 1532, 1344, 1272, 1261, 1217, 1157, 1142, 1124, 1057, and 1037 cm⁻¹ (Figure 1). The bands at 1532 and 1344 cm⁻¹ represent the antisymmetric and symmetric stretching modes, respectively, of the nitro group of the 1-(2-nitrophenyl)ethyl group which disappear during the formation of the *aci*-nitro anion intermediate (Scheme 3, A to B) (*13, 26, 27*). The band at 1272 cm⁻¹ represents the ν_a vibration of the γ-PO_2^- group of caged GTP, which also disappears in the caged GTP to *aci*-nitro anion intermediate transition. During formation of the *aci*-nitro intermediate, a proton is released (Scheme 3). Therefore, the bands at 1057 and 1037 cm⁻¹ (Figure 1) could indicate the protonation change of the MES buffer during the transition from caged GTP to the *aci*-nitro anion intermediate (Scheme 3, A to B), as these bands are missing in the spectrum of the *aci*-nitro anion decay. The intensities of the GTP bands at 1261, 1217, and 1157/1142 cm⁻¹ are different in the amplitude and photolysis difference spectrum due to overlaps with disappearing caged GTP bands. The positive band at 1124 cm⁻¹ (Figure 1) is only seen in the difference spectrum and not in the amplitude spectrum; therefore, this band is not attributed to the released GTP. Its assignment is not yet clear. Although Raman spectroscopic studies show an absorption at 1122 cm⁻¹, which is attributed
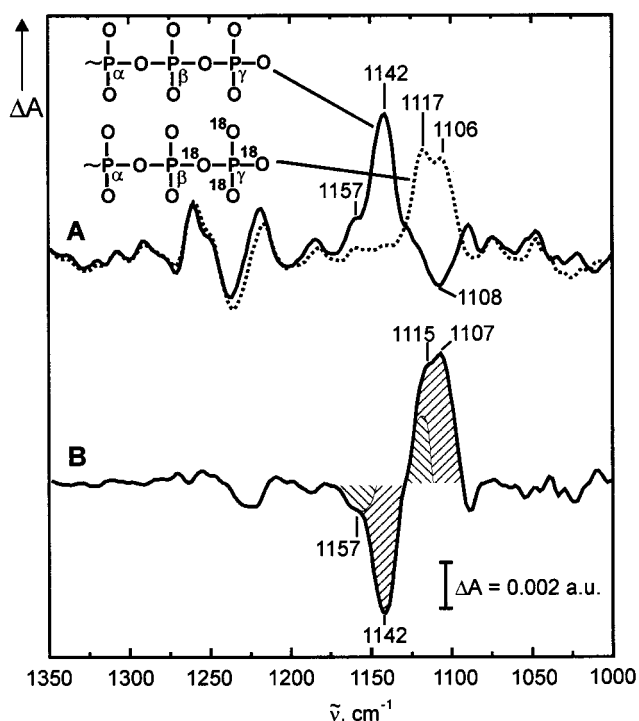

FIGURE 2: (A) Comparison of the photolysis amplitude spectra (B − C) of the Ras·GTP complex (—) and the γ-labeled Ras·GTP complex (···) and (B) difference between the labeled and unlabeled compound shown in trace A.

to the in-phase combination of GTP (*11*), we believe the band would be too weak to be detected in the IR.

For the assignment of the phosphate vibrations, ¹⁸O-labeled caged GTP was used. The substituted isotope lowers only the frequency of the vibration in which the labeled oxygen is involved. The amplitude difference spectra for unlabeled GTP and [β,γ-¹⁸O,γ-¹⁸O₃]GTP are shown only in the spectral region where phosphate bands are expected (Figure 2A). The photolysis amplitude spectra (Scheme 3, C − B), instead of the photolysis difference spectra (Scheme 3, C − A), are used for the assignments of the appearing GTP bands. The photolysis difference spectra are less suitable, because they contain strong disappearing caged GTP bands, which are sensitive to the isotope label and may mask shifted GTP bands. To visualize the band shifts due to isotopic labeling, differences between the amplitude spectra of the labeled and unlabeled isotopomers of GTP are calculated. The amplitude difference spectrum only contains the shifted bands (Figure 2B). Any other bands which are not affected by the labeling delete each other.

The comparison of the photolysis amplitude spectra of unlabeled GTP and [β,γ-¹⁸O,γ-¹⁸O₃]GTP (Figure 2A) shows a pronounced shift for product bands from 1157 and 1142 cm⁻¹ to 1117 and 1106 cm⁻¹, respectively. The dip between 1117 and 1106 cm⁻¹ is obviously caused by the negative band at 1108 cm⁻¹, which is superimposed on the down-shifted bands. The amplitude difference spectrum (Figure 2B) clearly exhibits a downshifted band from 1142 to 1107 cm⁻¹. Besides the main band at 1142 cm⁻¹, the small shoulder at 1157 cm⁻¹ is also downshifted to 1115 cm⁻¹ (Figure 2B). The band at 1142 cm⁻¹ can now be assigned to the $\nu_a(PO_3^{2-})$ vibration of the γ-phosphate group of GTP. A minor contribution of the $\nu_a(PO_3^{2-})$ vibration is seen at 1157 cm⁻¹ (Figure 2A,B). This minor part indicates that the PO_3^{2-}
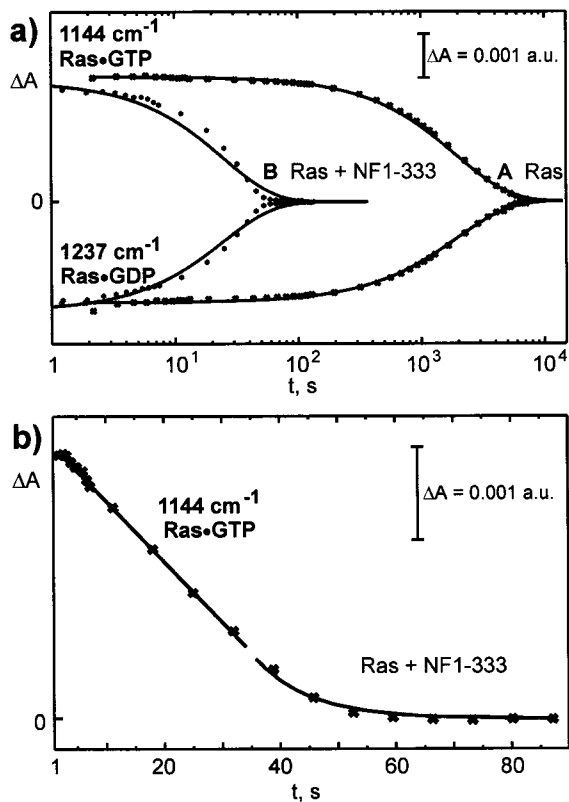
FIGURE 3: (a) Time course of IR marker bands at 1144 and 1237 cm^{-1}, indicating the disappearance of GTP and the appearance of GDP, the assessment of the GTPase reaction without NF1-333 at 310 K (A) and with catalytic amounts of NF1-333 at 283 K (B). The bands relax to zero because the Ras·GDP state is taken as a reference. (b) Time course of the GTPase reaction with a catalytic amount of NF1-333. The data of the first part are described by a linear function and the data of the second part by an exponential function.

vibrations are no longer degenerated. However, the γ-vibrations are highly localized, because no further pronounced band shift due to γ labeling is observed.

The photolysis difference spectra of the α and β labels are not shown. These labels will be presented and discussed in the context of the hydrolysis difference spectra below.

[α-^{18}O]/[γ-^{18}O]-mixed GTP labeling induces the same downshift of the bands at 1157/1142 cm^{-1} as the γ labeling alone but with weaker intensities (data not shown). In addition, the band at 1261 cm^{-1} (Figure 1) downshifts to 1241 cm^{-1}. Because this band is not observed in the measurement with [β,γ-^{18}O,γ-^{18}O$_3$]GTP, it must be caused by the α-^{18}O labeling. Therefore, the band at 1261 cm^{-1} is assigned to the ν_a(PO$_2^-$) vibration of the α-GTP.

(S_P)-[β-^{18}O]GTP and (R_P)-[β-^{18}O]GTP shift the band at 1217 to 1203 cm^{-1} (data not shown). The band at 1217 cm^{-1} (Figure 1) is therefore assigned to ν_a(PO$_2^-$) of β-GTP.

Hydrolysis of Ras·GTP. The intrinsic GTPase reaction was investigated in the presence of catalytic amounts of NF1-333 to accelerate the transition of the Ras·GTP intermediate to the Ras·GDP intermediate and P$_i$. In Figure 3a, the absorbance changes of marker bands for the hydrolysis reaction at 1144 and 1237 cm^{-1} are shown on a logarithmic time scale, with and without a catalytic amount of NF1-333. The absorbance changes are related to the final Ras·GDP state and therefore relax to zero. The two wavelengths represent the Ras·GTP and Ras·GDP states, respectively. A
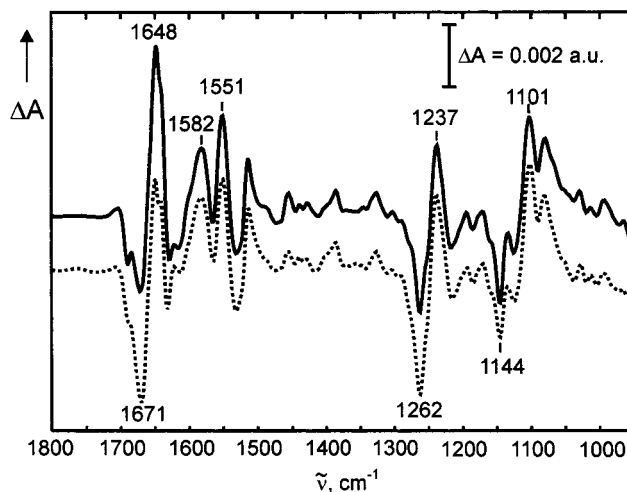

FIGURE 4: Comparison of difference spectra of the GTPase reaction with catalytic amounts of NF1-333 at 283 K (—) and without NF1-333 at 310 K (···).
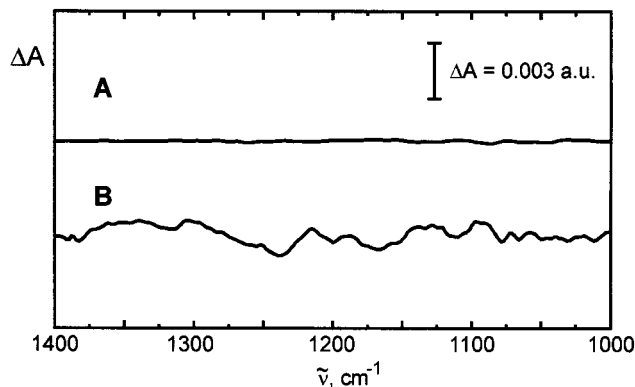

FIGURE 5: (A) Double difference between two hydrolysis difference spectra with unlabeled GTP from this work and (B) difference spectrum between two hydrolysis difference spectra with unlabeled GTP taken from ref *10*. They indicate the baseline stability.

global fit analysis, with one exponential ($k = 4.7 \times 10^{-4}$ s^{-1}), describes accurately the absorbance changes during the GTPase reaction, without NF1, at all wavenumbers. The GTPase is accelerated by 2 orders of magnitude with the catalytic amount of NF1-333 used. The absorbance changes with NF1-333 show deviations from exponential behavior due to the Michaelis−Menten dependence. This is obvious when the absorbance changes are presented on a linear time scale (Figure 3b). At the beginning, the concentration of the Ras·GTP substrate is very high compared to that of the NF1-333 enzyme. The absorbance, as a measure of the concentration, decreases linearly with time as expected for zero-order reactions. After ∼30 s, the amount of the Ras·GTP substrate is largely reduced and the concentration decreases approximately exponentially, as expected for first-order reactions, until, finally, the substrate is completely consumed.

In Figure 4, the hydrolysis difference spectra, with and without a catalytic amount of NF1-333, are compared. Both spectra exhibit the same difference bands (e.g., at 1671, 1648, 1582, 1551, 1262, 1237, 1144, and 1101 cm^{-1}) and agree well with the difference spectrum published by Cepus et al. (*10*). The quality of the baseline is shown in Figure 5A, where the control difference spectrum between two measurements with unlabeled samples in the phosphate region is presented. Before the subtraction, the spectra were normal-

ized to the bands between 1550 and 1300 cm^{-1}. To demonstrate the improvement in data quality, the corresponding control difference spectrum of Cepus et al. (*10*) is shown in Figure 5B. The improvement in baseline stability and signal-to-noise ratio is remarkable. Due to the shorter measuring time, baseline drifts caused by sample instabilities are largely reduced. The signal-to-noise ratio is further improved by using a vacuum FTIR instrument with an improved MCT detector.

For the assignment of the phosphate vibrations of the Ras·GTP intermediate and the Ras·GDP intermediate and P$_i$, the hydrolysis difference spectra of unlabeled GTP and [β,γ-$^{18}O,\gamma$-$^{18}O_3$]GTP are compared (Figure 6a, spectrum A). The former positive GTP product bands in the photolysis amplitude spectra (Figure 2A) now become negative educt bands in the hydrolysis difference spectra. As expected, the γ-GTP bands shift from 1157 and 1144 to around 1116 cm^{-1}. The double-difference spectrum reveals a shift from 1157 and 1143 to 1104 cm^{-1} (Figure 6b, spectrum A). An additional downshift is observed for two positive bands from 1078 to ~1053 cm^{-1} and, less obviously, from 992 to 973 cm^{-1} (compare spectra A in panels a and b of Figure 6). The positive bands, which are downshifted by the γ labeling (Figure 6a, spectrum A), must be caused by the released P$_i$ group.

To prove the P$_i$ assignment, experiments were performed in H$_2$^{18}O. An internal water molecule attacks the γ-phosphate in a nucleophilic manner and selectively introduces an ^{18}O label into the released P$_i$ (Scheme 1). The incorporated ^{18}O should shift the P$_i$ bands selectively. The hydrolysis difference spectrum (Figure 6a, spectrum B) and the double-difference spectrum (Figure 6b, spectrum B) exhibit a downshift from 1078 to 1053 cm^{-1} and a weaker shift from 992 to 973 cm^{-1}. The two bands are therefore assigned to P$_i$ vibrations.

Labeling the α and γ positions of GTP induces shifts at 1262, 1237, 1206, 1157, 1144, 1101, 1078, 1053, 992, and 973 cm^{-1} (Figure 6a, spectrum C). Due to γ labeling, the γ-phosphate vibrations are downshifted from 1157 and 1144 to around 1101 cm^{-1} and the P$_i$ vibration from 1078 to 1053 cm^{-1} and, less obviously, from 992 to 973 cm^{-1} (compare spectrum C in Figure 6a, spectrum C in Figure 6b, and spectrum A in Figure 6b). The shift of the negative educt band from 1263 to 1240 cm^{-1} in the double-difference spectrum and the shift of the positive band, superimposed on the band at 1240 cm^{-1}, from 1230 to 1207 cm^{-1} (Figure 6b, spectrum C) are missing in the spectrum with [β,γ-$^{18}O,\gamma$-$^{18}O_3$]GTP (spectra A in panels a and b of Figure 6). Therefore, the shift must be caused by the α labeling. The shifted product at the 1230 cm^{-1} band is highlighted by shading (Figure 6b, spectrum C). The band at 1262 cm^{-1} in the hydrolysis difference spectrum (Figure 6a, spectrum C) is assigned to the localized ν_a(PO$_2^-$) vibration of the α-phosphate of GTP. The positive band at 1237 cm^{-1} (Figure 6a, spectrum C) must be assigned to the ν_a(PO$_2^-$) vibration of the α-phosphate of GDP. The data clearly show that, in contradiction to Cepus et al. (*10*), a localized vibration at 1262 cm^{-1} can be assigned to the ν_a(α-PO$_2^-$) of GTP and a band at 1237 cm^{-1} to the ν_a(α-PO$_2^-$) of GDP.

The (S_P)-[β-^{18}O]GTP labeling shows effects on bands at 1216, 1204, 1144, 1124, 1101, and 1088 cm^{-1} (Figure 6a, spectrum D). The double-difference spectrum (Figure 6b,
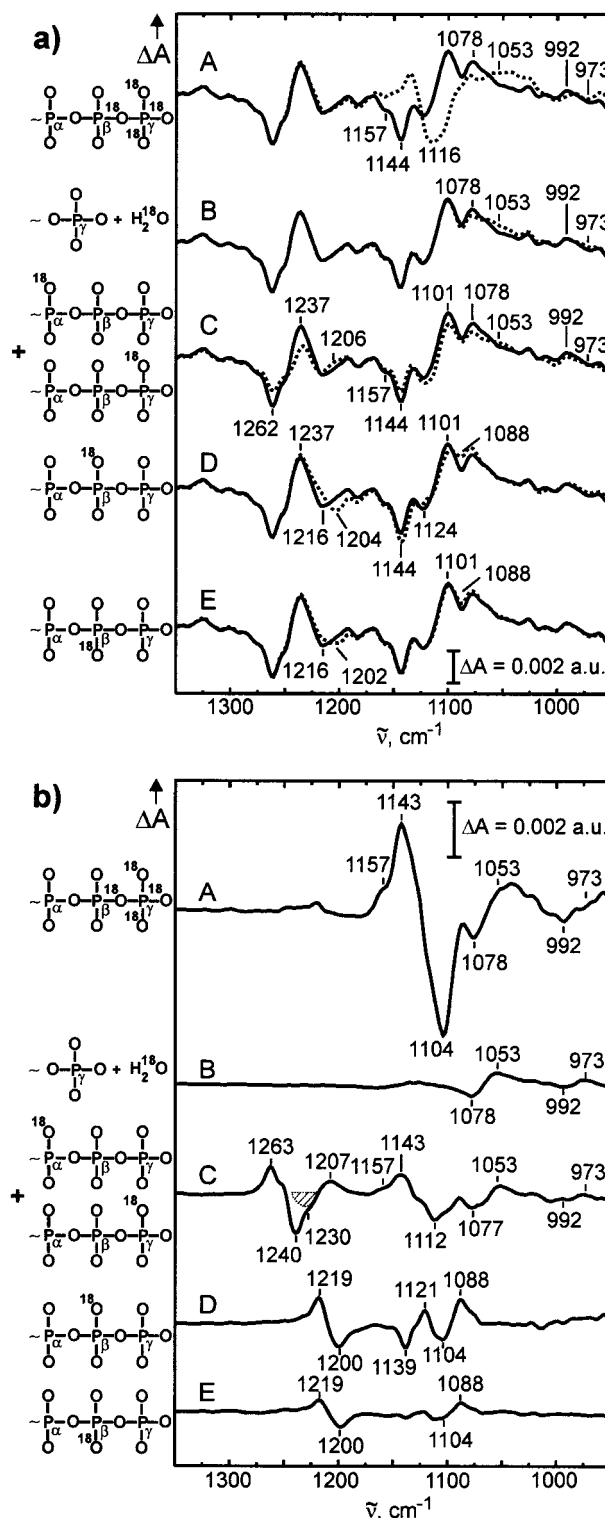

FIGURE 6: (a) Comparison of the hydrolysis difference spectra of the GTPase reaction at 283 K: (A) Ras·GTP (—) and Ras·[β,γ-$^{18}O,\gamma$-$^{18}O_3$]GTP (···), (B) Ras·GTP (—) and Ras·GTP in H$_2$^{18}O (···), (C) Ras·GTP (—) and Ras·[α-^{18}O]/[γ-^{18}O]GTP (···), (D) Ras·GTP (—) and Ras·(S_P)-[β-^{18}O]GTP (···), and (E) Ras·GTP (—) and Ras·(R_P)-[β-^{18}O]GTP (···). (b) Double-difference spectra of the hydrolysis difference spectra shown in panel a: (A) Ras·[β,γ-$^{18}O,\gamma$-$^{18}O_3$]GTP − Ras·GTP, (B) Ras·GTP in H$_2$^{18}O − Ras·GTP, (C) Ras·[α-^{18}O]/[γ-^{18}O]GTP − Ras·GTP, (D) Ras·(S_P)-[β-^{18}O]GTP − Ras·GTP, and (E) Ras·(R_P)-[β-^{18}O]GTP − Ras·GTP.

spectrum D) shows that an educt band shifts from 1219 to 1200 cm^{-1} and two product bands shift from 1139 and 1104 cm^{-1} to 1121 and 1088 cm^{-1}, respectively. The band at 1219

cm^{-1} is assigned to the $\nu_a(PO_2^-)$ of the β-phosphate group of GTP in the photolysis difference spectrum. The GDP bands at 1139 and 1104 cm^{-1} can be assigned to the appearing PO_3^{2-} group. The bands at 1139 and 1104 cm^{-1} are assigned to the two nondegenerated $\nu_a(PO_3^{2-})$ vibrations of the β-phosphate group of GDP.

In contrast to the results mentioned above, Cepus et al. (*10*) reported a band shift at 1239 cm^{-1} due to β labeling. However, the band shifts are only seen in the double-difference spectrum in Figure 5 of Cepus et al. (*10*). The effect in the double-difference spectrum can, instead of isotopic shifting, be caused by baseline instabilities which may lead to intensity variations at 1239 cm^{-1}. Since such a shift is not seen with the improved baseline stability in the measurements here (Figure 6a, spectra D and E), we attribute the effect seen by Cepus et al. to intensity variations between different samples.

(R_P)-[β-^{18}O]GTP shows an effect on the bands at 1216, 1202, 1101, and 1088 cm^{-1} (Figure 6a, spectrum E). The double-difference spectrum (Figure 6b, spectrum E) shows that an educt band shifts from 1219 to 1200 cm^{-1} and a product band shift from 1104 to 1088 cm^{-1}. The band shift from 1139 to 1121 cm^{-1} is not observed.

In summary, the assignments of the α-, β-, and γ-phosphate vibrations of GTP agree in general with the assignments given in Cepus et al. (*10*); however, the assignment attributed to the α-phosphate and P_i by Cepus et al. (*10*) must be modified. The α-labeled compound used by Cepus et al. shows shifts identical to those caused by the γ-labeled compound used here and is obviously mixed with γ-labeled material. Therefore, the assignment given by Cepus et al. for the α-vibration is incorrect. Furthermore, a detailed mass spectrometric analysis of the sample supposed to be "γ-^{18}O-labeled GTP" used by Cepus et al. showed that a [α-^{18}O]/[γ-^{18}O]-mixed labeled GTP was synthesized. In agreement, the same isotopic shifts are observed for this label here and in Cepus et al. (*10*). Therefore, the positive band at 1237 cm^{-1} in the hydrolysis difference spectra represents an α-GDP vibration and not, as assigned by Cepus et al., a P_i vibration. Furthermore, the pure γ label now indicates a localized vibration and not a delocalized vibration as concluded earlier by Cepus et al. from the mixed label.

DISCUSSION

Due to the improved quality of the FTIR data and the more precise determination of the labeled positions of GTP by ^{31}P nuclear magnetic resonance spectroscopy and electrospray mass spectrometry, as compared to those of Cepus et al. (*10*), the assignments of the Ras-bound GTP and GDP phosphate vibrations are now clear. The frequency downshifts due to isotopic labeling indicate isolated vibrations of single P–O bonds. Isotopic labeling shifts only the bands of the labeled group, but not bands of other groups as would be expected for coupled vibrations. Because the vibrations are mainly uncoupled, a straightforward explanation of the observed frequency shifts can be given.

The band assignments are summarized in Figure 7a. In addition, the wavenumbers of absorption bands of free GTP, GTP·Mg^{2+}, free GDP, GDP·Mg^{2+} (*28*), and HPO$_4^{2-}$ (*26*, *29*) are listed. Thereby, the frequency shifts due to protein binding are better visualized.

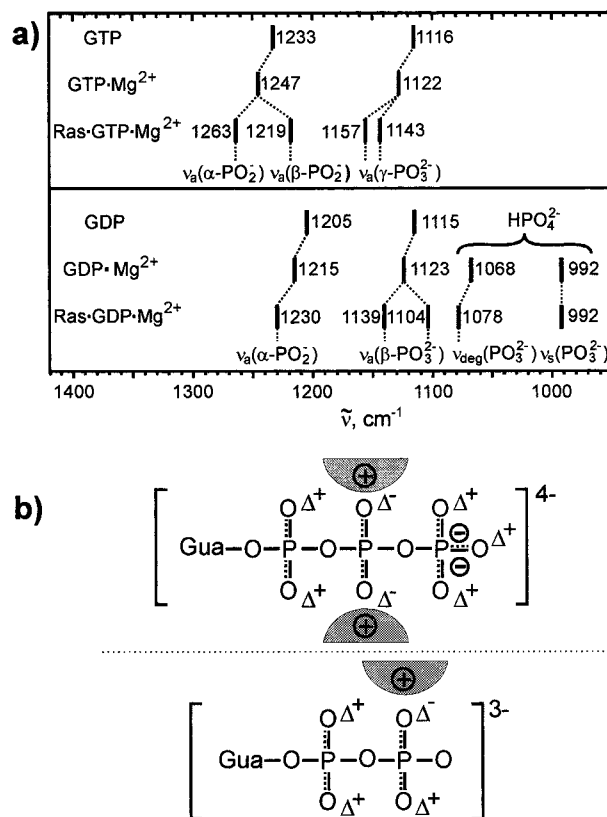FIGURE 7: (a) Comparison of the frequencies of the phosphate bands of GTP, GTP·Mg^{2+}, and Ras-bound GTP·Mg^{2+} and of GDP, GDP·Mg^{2+}, and Ras-bound GDP·Mg^{2+}. The listed wavenumbers of Ras·GTP, Ras·GDP, and P_i correspond to the band positions in the hydrolysis double-difference spectra. The frequencies for GTP, GTP·Mg^{2+}, GDP, and GDP·Mg^{2+} are taken from ref *28*, and that for HPO$_4^{2-}$ is taken from refs *26* and *29*. (b) Induced charge shifts Δ of GTP and GDP by Ras binding as deduced from the frequency shifts.

The α- and γ-GTP vibrations are upshifted due to Mg^{2+} and Ras binding, whereas the β-GTP vibrations are downshifted (Figure 7a). The γ-PO$_3^{2-}$ vibration is no longer degenerate and splits into two vibrations. The α-GDP vibration is upshifted. The Ras·β-GDP vibration is also no longer degenerate and splits on binding into an upshifted and downshifted vibration.

What can be learned from the IR frequency shifts due to Ras binding? In general, the IR frequencies are determined by the bond order, the mass, the geometry, and the coupling between the normal modes of the vibrating groups. To determine from the frequencies the electron distribution and the geometry of the vibrating groups, ab initio quantum chemical calculations of the complete vibrating Ras·GTP system are most appropriate. However, at present, only molecules the size of GTP can be calculated ab initio. On the other hand, the frequency shifts due to protein binding indicate that the interaction of GTP with the protein in the binding pocket cannot be neglected. Therefore, the ab initio calculations of GTP alone match the observed frequencies only within ∼10% (*11*). This is a larger deviation than the observed shifts due to binding. Therefore, the ab initio calculations can only be used to propose the tendency of frequency shifts due to putative interactions.

Fortunately, the vibrations are highly localized as pointed out, and to a first approximation, the complete vibrating system does not have to be considered. The observed
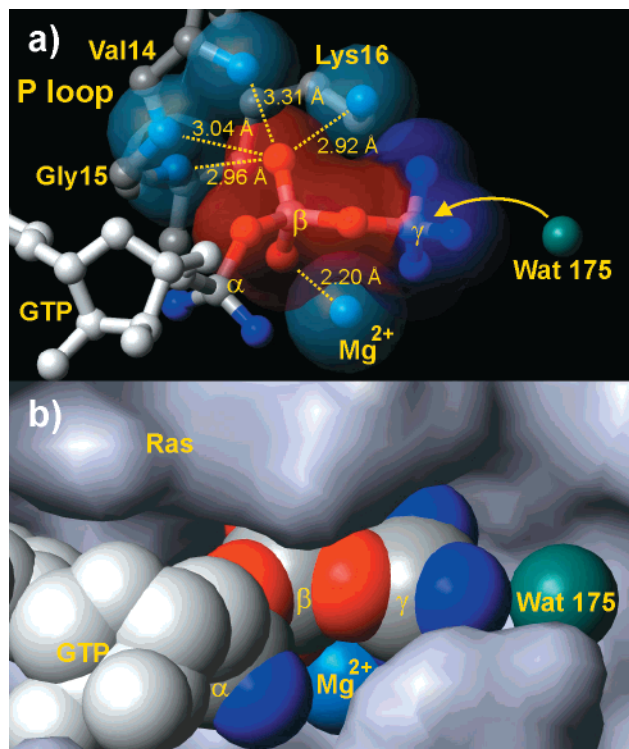
FIGURE 8: (a) Charge shifts of GTP due to Ras binding as deduced from the FTIR data. Blue indicates positive charges, and red indicates negative charge. On the basis of the crystallographic structural model (*4*), mainly Mg^{2+} appears to pull negative charges toward the *pro-R* oxygen and mainly the protein backbone NHs of Lys 16, Gly 15, Val 14 of the structural highly conserved P loop appear to pull charges toward the *pro-S* oxygen. Especially, the Lys 16 side chain also contributes. The charge shifts facilitate the cleavage of the $\beta-\gamma$ bridging bond. This is now recognized as a key element contributing to catalysis. (b) Same view as in panel a, but now the complete protein surface in which GTP is embedded is shown.

frequency shifts report directly on the properties of the individual vibrating groups. An influence on the frequency shifts due to larger geometric changes is unlikely, because the X-ray data do not show larger structural changes due to Ras binding. Therefore, the frequency shifts of the protein-bound GTP and GDP phosphate vibrations report mainly on bond order changes of the involved local vibrating groups. A frequency upshift indicates a stronger force constant due to a bond order increase, whereas a downshift indicates a bond order decrease. The bond order changes can then be related to specific interactions of individual GTP and GDP phosphate groups with the binding pocket.

The α-GTP phosphate vibration is upshifted by 16 cm^{-1} to 1263 cm^{-1}. This shows an increased bond order for the α-PO$_2^-$ group in the protein as compared to GTP·Mg^{2+} in solution. According to the crystal structural model, the α-PO$_2^-$ phosphate group interacts with the main chain amide of Ser 17 and Ala 18 and with three water molecules (*4*). The upshift indicates less H-bonding than in solution, which leads to a decrease in negative charge at the nonbridging α-oxygens upon protein binding (Figures 7b and 8).

The $\nu_a(\beta$-PO$_2^-)$ of GTP is downshifted by 28 cm^{-1} to 1219 cm^{-1} for *pro-S* and *pro-R* ^{18}O labeling as compared to GTP·Mg^{2+}. This indicates a bond order decrease for the *pro-R* and *pro-S* nonbridging P−O bonds of the β-phosphate upon protein binding. The X-ray structural model proposes that

the *pro-R* oxygen coordinates with the bound Mg^{2+} (*4*). Usually, the phosphate vibrations of nucleotides are upshifted on coordination with divalent cations in solution (*28, 30, 31*). The positive Mg^{2+} charge appears to induce a $\pi(p-d)$ bond for the noncoordinated P−O group, which increases the bond order of the noncoordinated group. Consequently, the bond order of the coordinated P−O group should decrease. In agreement, *pro-S* and *pro-R* exhibit different bond orders for free GTP·Mg^{2+} (unpublished results). The decrease in both nonbridging β P−O bond orders due to protein binding can be explained by the strong symmetric interaction of both oxygens with the protein, which pulls electrons toward both oxygens and thereby weakens both P−O bonds. Thus, more negative charge accumulates at both nonbridging β oxygens upon protein binding (Figure 7b). Very likely candidates in the structural model providing stronger interaction with the *pro-S* oxygen are the NH groups of Lys 16, Gly 15, and Val 14 and possibly the side chain of Lys 16 (*4*). These amino acids are part of the structurally highly conserved P loop of G-proteins (*8*). The correct positioning of the backbone amide groups of Lys 16, Gly 15, and Val 14 respective to GTP seems therefore to be crucial for the catalysis provided by Ras, in addition to Mg^{2+}. Site-directed mutations, which influence the correct position of the P loop, influence indirectly the hydrolysis rate.

A major part of the GTP γ-phosphate vibration is upshifted by 21 cm^{-1} to 1143 cm^{-1} and a minor part by 35 cm^{-1} to 1157 cm^{-1} as compared to free GTP·Mg^{2+}. This indicates a bond order increase and more H-bonding than in solution. Ab initio calculations show that this vibration is insensitive to the position of the metal ion, which is reasonably close to that found in the structural model (*11*). In addition, the influence of structural changes, such as an increase in the angle between the nonbridging P−O bonds of the γ-phosphate and different positioning of the attacking water 175 on the position of the $\nu_a(\gamma$-PO$_3^{2-})$ vibration, was investigated by ab initio calculations (*11*). The calculations do not predict such large shifts for the $\nu_a(\gamma$-PO$_3^{2-})$ vibration as observed. Therefore, geometric effects and the position of water 175 do not seem to contribute largely to the experimentally observed frequency shifts. They seem to be mostly caused by bond order changes. The bond order increase reflects the decrease in negative charge at the γ oxygens in the protein as compared to solution (Figures 7b and 8a). A minor part of the γ-phosphate vibration is upshifted to 1157 cm^{-1}. This indicates that the symmetry of the γ-PO$_3^{2-}$ group, which leads to degeneracy for unbound GTP, is disturbed in the protein-bound case. For a C_{3v} symmetry of the PO$_3^{2-}$ group, a degenerate vibration is expected. The protein interaction appears to disturb this symmetry significantly. Alternatively, two different conformations of the γ-phosphate group could also explain the two bands.

For GDP, the α-PO$_2^-$ vibration is upshifted similarly to GTP. This indicates a similar interaction of the α-phosphate group in GTP and GDP with the protein. This is expected from the structural models of the Ras·GTP and Ras·GDP complexes.

The GDP β-PO$_3^{2-}$ vibration is also not degenerate. In contrast to the PO$_3^{2-}$ vibrations of GTP, the two vibrations show equivalently strong bands. One vibration absorbs like the γ-PO$_3^{2-}$ vibrations at 1139 cm^{-1}, whereas the other one is downshifted to 1104 cm^{-1}. The band at lower wave-

numbers mostly represents a PO_2^- group still strongly bound to the protein, like β-PO_2^-. The band at higher wavenumbers seems to represent mostly the third least bound P—O group in the hydrophobic protein environment like γ-PO_3^{2-}. So there is an asymmetric electronic distribution in the β-PO_3^{2-} group. The conclusion is similar to the one made by Cepus et al. (*10*). Alternatively, as for γ-PO_3^{2-}, two different conformations of β-PO_3^{2-} could explain the band splitting.

Further, it can be concluded that during the hydrolysis of GTP the Mg^{2+} remains bound to the β-phosphate oxygen of GDP which arises from the β *pro-S* oxygen of GTP. If the β-phosphate group of GDP could rotate, and the oxygens interacted in a random distribution with the metal ion, the (R_P)- and (S_P)-diastereomeres would yield the same spectra, but they are quite different.

The released P_i exhibits bands at 1078 and 992 cm^{-1}. These two vibrations are indicative of HPO_4^{2-}, which absorbs at 1068 [$\nu_{deg}(PO_3^{2-})$] and 992 cm^{-1} [$\nu_s(PO_3^{2-})$], respectively. This is surprising, because at pH 6 an $H_2PO_4^-$ species is expected. However, its characteristic band at 947 cm^{-1} (*29*) does not appear in the hydrolysis difference spectra, therefore excluding its presence. Interestingly, for a dissociative mechanism, an HPO_4^{2-} species is expected immediately after the cleavage, whereas for the associative mechanism proposed by Schweins et al. (*32*), an $H_2PO_4^-$ species is expected (Scheme 1). Nevertheless, the equilibrium of the orthophosphates could be largely shifted toward HPO_4^{2-} by Mg^{2+} in the bulk phase (*33*).

In summary, the frequency shifts indicate a decrease in negative charge at oxygens and an increase in negative charge at the β oxygens in the GTP and GDP state due to specific interactions with the protein. To deduce from the IR frequencies the exact charge distribution, QM/MM hybrid calculations are in progress (*34*, *35*). However, there is a relationship for PO_2^- groups between the force constant and the ν_a established by Pohle et al. (*36*). On the basis of this rough estimation, the force constant for the β-PO_2^- GTP group would decrease upon protein binding by about 5% relative to that of free GTP·Mg^{2+}. Even if these changes are small, they appear to contribute significantly to catalysis. It has to be considered that the protein is a soft, highly fluctuating polymer which induces alteration of the charge distribution in the much more rigid GTP. The detection of such small changes is outside the realm of X-ray diffraction, but they are large enough to channel the reaction pathway leading to catalysis.

For a dissociative mechanism, the observed charge shift from the γ- to β-phosphate is the expected direction of the electron movements in the transition state (*9*). The distribution of negative charges for a dissociative and an associative transition state is quite different (Scheme 1). For a dissociative transition state, most negative charge resides on the β-phosphate, whereas for an associative transition state, negative charge is accumulated mainly on the γ-phosphate (Scheme 1). Even though the transition state itself is not monitored in the hydrolysis difference spectra, it is unlikely that the protein undergoes larger structural changes only in the transition state which completely alter the charge distribution pattern, and then resets these structural changes back again to their original position in the GDP state. Therefore, the pattern of charge distribution in the transition

state is unlikely to be dramatically altered as compared to those of Ras·GTP and Ras·GDP.

However, independent of the occurrence of a dissociative or an associative transition state, charge finally has to be moved from the γ-PO_3^{2-} group to the β-PO_3^{2-} group during hydrolysis (Scheme 1). By the protein-induced charge shift, the charge distribution in the GTP educt state is already GDP-like. This is a factor in lowering the activation energy of the transition state.

In the GAP-catalyzed reaction, it is conceivable that the mechanism changes in a fundametal manner. Additional interactions between GAP and Ras-bound GTP may change the charge distribution. An arginine from GAP is proposed to catalyze the hydrolysis reaction, and this has been confirmed by mutational analysis of NF1-333 (*37*). This additional positive charge close to the γ-phosphate, as deduced from the putative GDP·AlF_3 or GDP·AlF_4^- transition state analogues (*38*), will have significant influence on the charge distribution. The GAP-catalyzed mechanism has been investigated in a further FTIR study (C. Allin, M. R. Ahmadian, A. Wittinghofer, and K. Gerwert, manuscript submitted for publication).

After completion of this work, we became aware of two relevant publications (*12*, *39*). Du et al. (*12*) followed the experimental approach introduced by Cepus et al. (*10*), time-resolved FTIR difference spectroscopy in combination with isotopically labeled caged GTP. They confirm the band assignments of Cepus et al. and incorporated the assignments of the Raman study by Wang et al. (*11*). Overall, the assignments agree well, except the $\nu_a(PO_2^-)$ α-GTP and $\nu_a(PO_3^{2-})$ β-GDP vibrations. Here, we have elaborated that in the synthesis used not only the γ-phosphate group, as thought by Cepus et al., but surprisingly also the α-phosphate group of GTP is labeled. This now solves the small discrepancy in the independently performed band assignments in the two former publications. The assignments performed in this paper and by Du et al. are in excellent agreement. This is an impressive conformation of the power of site-directed isotopic labeling for clear-cut band assignments. On the basis of the band assignments, Du et al. (*12*) came to the same conclusion as did Cepus et al. (*10*), i.e., that the intrinsic GTPase reaction has substantial dissociative character, and propose in agreement a concerted mechanism.

On the other hand, Due et al. contradict the proposal by Cepus et al. that the frequency shift of the $\nu_a(PO_2^-)$ β-GTP vibration correlates with the hydrolysis rate. They argue that the frequency shifts observed in several site-directed mutants do not correlate with their hydrolysis rate. However, our unpublished data show between 1800 and 1350 cm^{-1}, a spectral region not presented by Du et al., large deviations in these regions between mutant and wild type difference spectra. This indicates that the mutations are too invasive to be simply compared to the wild type, as done by Du et al. The mutations used might affect other factors contributing to catalysis, such as the exact positioning of the attacking water. We have recently completed a study showing a linear correlation between the frequency shift, indicative for the charge movement toward β-phosphate, and the hydrolysis rate (M. Blessenohl, C. Allin, and K. Gerwert, unpublished results).

Glennon et al. (*39*) have simulated the GTPase reaction using the empirical valence bond method. They showed that a shift of negative charge toward the β-phosphate of GTP by electrostatic interaction with Ras and GAP accelerates the hydrolysis. This is in line with our proposal that the shift of negative charge from the γ-phosphate toward the β-phosphate already present in GTP bound by Ras is a key element in catalysis.

ACKNOWLEDGMENT

REFERENCES

1. Barbacid, M. (1987) *Annu. Rev. Biochem. 56*, 799−827.
2. Ahmadian, M. R., Hoffmann, U., Goody, R. S., and Wittinghofer, A. (1997) *Biochemistry 36*, 4535−4541.
3. Wittinghofer, A., Scheffzek, K., and Ahmadian, M. R. (1997) *FEBS Lett. 410*, 63−67.
4. Pai, E. F., Krengel, U., Petsko, G. A., Goody, R. S., Kabsch, W., and Wittinghofer, A. (1990) *EMBO J. 9*, 2351−2359.
5. Tong, L., de Vos, A. M., Milburn, M. V., and Kim, S.-H. (1991) *J. Mol. Biol. 217*, 503−516.
6. Schlichting, I., Almo, S. C., Rapp, G., Wilson, K., Petratos, K., Lentfer, A., Wittinghofer, A., Kabsch, W., Pai, E. F., Petsko, G. A., and Goody, R. S. (1990) *Nature 345*, 309−315.
7. Scheidig, K. A. J., Burmester, C., and Goody, R. S. (1999) *Structure 7*, 1311−1324.
8. Kjeldgaard, M., Nyborg, J., and Clark, B. F. C. (1996) *FASEB J. 10*, 1347−1368.
9. Maegley, A., Admiraal, S. J., and Herschlag, D. (1996) *Proc. Natl. Acad. Sci. U.S.A. 93*, 8160−8166.
10. Cepus, V., Scheidig, A. J., Goody, R. S., and Gerwert, K. (1998) *Biochemistry 37*, 10263−10271.
11. Wang, J. H., Xiao, D. G., Deng, H., Webb, M. R., and Callender, R. (1998) *Biochemistry 37*, 11106−11116.
12. Du, X., Frei, H., and Kim, S.-H. (2000) *J. Biol. Chem. 275*, 8492−8500.
13. Walker, A. W., Reid, G. P., McCray, J. A., and Trentham, D. R. (1988) *J. Am. Chem. Soc. 110*, 7170−7177.
14. Tucker, J., Sczakiel, G., Feuerstein, J., John, J., Goody, R. S., and Wittinghofer, A. (1986) *EMBO J. 5*, 1351−1358.
15. Hoard, E., and Ott, D. G. (1965) *J. Am. Chem. Soc. 87*, 1785−1793.
16. Hecht, S. M., and Kozarich, J. W. (1973) *Biochim. Biophys. Acta 331*, 307−309.
17. Connolly, B. A., Eckstein, F., and Füldner, H. H. (1982) *J. Biol. Chem. 257*, 3382−3384.
18. Kalbitzer, H. R., Feuerstein, J., Goody, R. S., and Wittinghofer, A. (1990) *Eur. J. Biochem. 188*, 355−359.
19. Walker, J. W., Reid, G. P., and Trentham, D. R. (1989) *Methods Enzymol. 172*, 288−301.
20. Glonek, T., Kleps, R. A., and Myers, T. C. (1974) *Science 185*, 352−355.
21. Webb, M. R. (1980) *Biochemistry 19*, 4744−4748.
22. John, J., Schlichting, I., Schiltz, E., Rösch, P., and Wittinghofer, A. (1989) *J. Biol. Chem. 264*, 13086−13092.
23. Gerwert, K., Souvignier, G., and Hess, B. (1990) *Proc. Natl. Acad. Sci. U.S.A. 87*, 9774−9778.
24. Souvignier, G., and Gerwert, K. (1992) *Biophys. J. 51*, 627−635.
25. Hessling, B., Souvignier, G., and Gerwert, K. (1993) *Biophys. J. 65*, 1929−1941.
26. Cepus, V., Ulbrich, C., Allin, C., Troullier, A., and Gerwert, K. (1998) *Methods Enzymol. 291*, 223−245.
27. Barth, A., Corrie, J. E. T., Gradwell, M. J., Maeda, Y., Mäntele, W., Meier, T., and Trentham, D. R. (1997) *J. Am. Chem. Soc. 119*, 4149−4159.
28. Wang, J. H., Xiao, D. G., Deng, H., Callender, R., and Webb, M. R. (1998) *Biospectroscopy 4*, 219−227.
29. Chapman, A. C., and Thirlwell, L. E. (1964) *Spectrochim. Acta 20*, 937−947.
30. Brintzinger, H. (1963) *Biochim. Biophys. Acta 77*, 345−348.
31. Takeuchi, H., Murata, H., and Harada, I. (1988) *J. Am. Chem. Soc. 110*, 392−397.
32. Schweins, T., Geyer, M., Kalbitzer, H. R., Wittinghofer, A., and Warshel, A. (1996) *Biochemistry 35*, 14225−14231.
33. Taylor, A. W., Frazier, A. W., Gurney, E. L., and Smith, J. P. (1967) *Trans. Faraday Soc. 59*, 1585−1589.
34. Car, R., and Parrinello, M. (1985) *Phys. Rev. Lett. 55*, 2471−2474.
35. Eichinger, M., Tavan, P., Hutter, J., and Parinello, M. (1999) *J. Chem. Phys. 110*, 10452−10467.
36. Pohle, W., Bohl, M., and Böhlig, H. (1990) *J. Mol. Struct. 242*, 333−342.
37. Ahmadian, M. R., Stege, P., Scheffzek, K., and Wittinghofer, A. (1997) *Nat. Struct. Biol. 4*, 686−689.
38. Scheffzek, K., Ahmadian, M. R., Kabsch, W., Wiesmüller, L., Lautwein, A., Schmitz, F., and Wittinghofer, A. (1997) *Science 277*, 333−338.
39. Glennon, T. M., Villà, J., and Warshel, A. (2000) *Biochemistry 39*, 9641−9651.